HHS Public Access

Author manuscript

J Orthop Res. Author manuscript; available in PMC 2020 November 01.

Published in final edited form as:

J Orthop Res. 2019 November ; 37(11): 2476–2485. doi:10.1002/jor.24397.

Non-invasive ultrasound quantification of Scar Tissue Volume identifies early functional changes during tendon healing.

Jessica E. Ackerman[1], **Valentina Studentsova**[1], **Marlin Myers**[1], **Mark R. Buckley**[1,2], **Michael S. Richards**[3], **Alayna E. Loiselle**[1,*]

[1]Center for Musculoskeletal Research, Department of Orthopaedics & Rehabilitation, University of Rochester, Rochester, New York, United States of America

[2]Department of Biomedical Engineering, University of Rochester, Rochester, New York, United States of America

[3]Department of Biomedical Engineering, Rochester Institute of Technology, Rochester, New York, United States of America

Abstract

Tendon injuries are very common and disrupt the transmission of forces from muscle to bone, leading to impaired function and quality of life. Successful restoration of tendon function after injury is a challenging clinical problem due to the pathological, scar-mediated manner in which tendons heal. Currently, there are no standard treatments to modulate scar tissue formation and improve tendon healing. A major limitation to the identification of therapeutic candidates has been the reliance on terminal end-point metrics of healing in pre-clinical studies, which require a large number of animals and result in destruction of the tissue. To address this limitation, we have identified quantification of Scar Tissue Volume (STV) from ultrasound imaging as a longitudinal, non-invasive metric of tendon healing. STV was strongly correlated with established endpoint metrics of gliding function including Gliding Resistance (GR) and Metatarsophalangeal (MTP) Flexion Angle. However, no associations were observed between STV and structural or material properties. To define the sensitivity of STV to identify differences between functionally discrete tendon healing phenotypes, we utilized S100a4 haploinsufficient mice ($S100a4^{GFP/+}$), which heal with improved gliding function relative to wildtype (WT) littermates. A significant decrease in STV was observed in $S100a4^{GFP/+}$ repairs, relative to WT at day 14. Taken together, these data suggest US quantification of STV as a means to facilitate the rapid screening of biological and pharmacological interventions to improve tendon healing, and identify promising therapeutic targets, in an efficient, cost-effective manner.

Keywords

tendon healing; ultrasound; scar tissue; mouse model; range of motion

*Corresponding Author Alayna E. Loiselle, PhD, Center for Musculoskeletal Research, University of Rochester Medical Center, 601 Elmwood Ave, Box 665, Rochester, NY, 14642, Phone: 585-275-7239, Fax: 585-276-2177, Alayna_Loiselle@urmc.rochester.edu.

Author Contributions:

Study conception and design: JEA, AEL; Acquisition of data: JEA, VS, MM; Analysis and interpretation of data: JEA, VS, MRB, MSR, AEL; Drafting of manuscript: JEA, AEL; Revision and approval of manuscript: JEA, VS, MM, MRB, MSR, AEL.

Introduction

Tendon injuries, including traumatic transections and ruptures due to tendon degeneration, disrupt the transmission of forces from muscle to bone, leading to chronic pain, disability and a large socioeconomic burden[1]. Tendon injuries are very common, as there are over 300,000 tendon repair procedures a year in the United States[2], which result from either acute trauma or chronic tendinopathy. While satisfactory outcome rates vary between different tendons, successful restoration of tendon function after injury remains a challenging clinical problem, with up to 40% of flexor tendon injuries healing with functional limitations[3]. Unsatisfactory outcomes of surgical tendon repair procedures are due to the pathological, scar-mediated manner in which tendons heal. Rather than regenerating native tendon tissue, tendons heal via bridging scar tissue composed of a disorganized collagen extracellular matrix (ECM), resulting in mechanical properties that are inferior to native tendon, and increasing the risk of re-injury or rupture. Additionally, scar tissue impairs tendon range of motion (ROM), a particularly problematic complication in the flexor tendons of the hands[3].

Despite attempts using a variety of biological and tissue engineering approaches, there is currently no consensus therapy to improve outcomes after tendon injury. An insufficient understanding of the underlying mechanisms that contribute to scar-mediated tendon healing is a major impediment to the development of successful therapies. To address this limitation, we developed a murine model of tendon injury and repair that recapitulates many clinical aspects of healing including abundant scar tissue formation and impaired restoration of mechanical properties [4]. However, progress in this field is limited by the absence of cost-effective longitudinal outcome measures of tendon healing. Currently, we quantify impairments in gliding function using end-point analyses of Gliding Resistance and measurement of the Metatarsophalangeal (MTP) flexion angle after loading of the proximal FDL with small weights[4,5], consistent with large animal[6] and cadaveric studies[7]. This powerful technique has allowed us to define the temporal course of scar formation in the murine model[4], and demonstrated the effects of genetic and pharmacological perturbations on the healing process [8,9]. However, these studies require many animals to properly power the study and to get sufficient temporal resolution over the course of scar formation and healing. Thus, current approaches are expensive, time-consuming and do not allow longitudinal evaluation or concomitant assessment of function and tissue morphology in the same specimen. Therefore, our objective was to establish quantification of Scar Tissue Volume from high-frequency ultrasound (US) images as a longitudinal, non-invasive metric of tendon healing. US-based quantification of tendon function will dramatically reduce the number of animals needed by longitudinally assessing a single cohort of animals over the entire course of healing. Furthermore, US-based characterization will provide more flexibility as we characterize novel genetic models and interventions as we can image at many more time-points. In addition, while GR and MTP Flexion allow us to make assumptions about tissue morphology, concomitant assessment of function and morphology are not possible in a single specimen. In contrast, 3D reconstruction and segmentation of US images allow direct assessment and quantification of tissue morphology. Finally, US is an ideal modality to longitudinally assess tendon healing, as it is non-ionizing, and can be easily scaled between pre-clinical and clinical applications.

Methods

Animal Ethics:

This study was carried out in strict accordance with the recommendations in the Guide for the Care and Use of Laboratory Animals of the National Institutes of Health. All animal procedures were approved by the University Committee on Animal Research (UCAR) at the University of Rochester (UCAR Number: 2014–004).

Acute tendon injury and repair:

Mice were group-housed (up to 5 mice per cage) under standard conditions with a 12hr/12hr light/dark cycle. The following strains of mice were obtained from Jackson laboratories (Bar Harbor, ME): C57BL6/J (#664) and S100a4$^{GFP/+}$ and Wildtype (WT) littermates (#012904; B6.129S6-*S100a4*^{tm1Egn}/YunkJ). Only female C57Bl/6J mice were used (weight: 20.61g ± 1.24), while male and female S100a4$^{GFP/+}$ and WT mice were used in equal proportions across genotypes (weight: S100a4$^{GFP/+}$ males: 26.7g ± 1.81; S100a4$^{GFP/+}$ females: 20.7g ± 0.99; WT males: 24.4g ± 0.85; WT females: 20.02g ± 1.29). At 10–12 weeks of age, mice underwent surgical transection and repair of the flexor digitorum longus (FDL) tendon in the hind paw, using a modified Kessler suture technique, as we have previously described [4]. Mice were anesthetized with Ketamine (100mg/kg)/ Xylazine (10mg/kg). Pre-operative sustained-release Buprenorphine (1mg/kg) analgesia was also administered. Following sedation, the distal FDL tendon was exposed and transected; two horizontal 8–0 sutures were placed in the intact tendon ends and the tendon was sutured to approximate an end-to-end repair. The tendon was also transected proximally along the tibia at the myotendinous junction to decrease strain on the repair.

Ultrasound quantification of Scar Tissue Volume:

A high-frequency ultrasound platform (Vevo® 3100, FUJIFILM VisualSonics Inc., Toronto, Canada), with a 70-MHz transducer probe (MX700; FUJIFILM VisualSonics Inc., Toronto, Canada) was used for *in vivo* imaging of the healing tendon. The MX700 provides and axial resolution of 30μm and a lateral resolution of 65μm. For imaging studies, mice were anesthetized with isoflurane, and placed in the prone position. The right hind paw was gently secured proximal to tibiotalar (ankle) joint with surgical tape, such that no additional strain was placed on the tendon. After aligning the ultrasound probe with the tendon at the mid-point of the hind paw, the hind paw was covered in ultrasound gel (Aquasonic 100, Parker, Fairfield, NJ) and imaged. A total of 105 40μm-thick sagittal B mode images were collected across the 4mm region of interest (ROI), which included the entire width of the hind paw. All system settings, including gain (96%), monitor dynamic range (70 dB), and depth (2 cm), were kept constant. Echogenicity was quantified in a rectangular region of interest in the middle of the scar tissue from greyscale images using NIH Image J software. Each pixel had a grey scale value between 0–255 (0=black, 255=white), and the average intensity (echogenicity) of the ROI was calculated for each specimen.[10,11]

The same cohort of mice (n=9) underwent ultrasound imaging at 7, 14, 20, and 28 days post-surgery, followed by assessment of gliding function and mechanical properties at day 28 (Figure 1A). Two mice were excluded from analysis at day 28 due to failure during testing.

An additional cohort of animals (n=7) underwent ultrasound imaging at day 14, followed by sacrifice and assessment of gliding function and mechanical properties.

Segmentation and validation with histology:

B-mode images were exported as 3D volumes and loaded in to AMIRA (FEI v.6.1.1, Thermo Scientific, Hillsboro, OR). The scar tissue boundaries were identified and manually segmented on each slice. A 3D reconstruction of the scar tissue was generated and volumetrically quantified, resulting in the Scar Tissue Volume (STV) metric. To validate the correct segmentation of STV in US images, a subset of specimens (n=5) underwent both US imaging and histological evaluation. Following US imaging, mice were sacrificed, and hind paws were harvested and fixed in 10% neutral buffered formalin (NBF) for 72 hours at room temperature. Samples were then decalcified for 7 days in 14% EDTA[12] at room temperature and processed for paraffin histology. Serial 5μm sagittal sections were cut through the entire width of the hind paw that included the flexor tendon and/or scar tissue. For 3D reconstruction, sections corresponding to every 40μm were stained with Alcian Blue/ Hematoxylin/ Orange G (ABHOG), as the step size of the US images was 40μm. ABHOG was used as it allows easy discrimination between native tendon and scar tissue [8]. Stained sections were then digitally imaged, aligned, and stacked using NIH Image J [13], and loaded in to AMIRA. Scar tissue was then manually segmented in each slice, and volumetrically quantified.

Assessment of Gliding Function, Mechanical Testing and Calculation of Material Properties:

Following ultrasound imaging, C57Bl/6J mice were sacrificed at day 14 or day 28 post-surgery (n=7 per time-point), while S100a4$^{GFP/+}$ and wildtype (WT) littermates were harvested at day 14 (n=12–14) for assessment of gliding function and tensile mechanical testing [4,5]. The hindlimb was disarticulated at the knee and the skin was removed down to the ankle. The FDL tendon was isolated at the myotendinous junction and secured between two pieces of tape. The tibia was gripped in an alligator clip and the FDL was incrementally loaded with small weights from 0–19g. Digital images were taken after each weight was applied and the flexion angle at the metatarsophalangeal (MTP) joint was measured from these images. The MTP Flexion angle corresponds to the difference in flexion from the neutral, unloaded (0g) image, and the flexion angle when the 19g weight is applied. Application of a 19g weight results in complete flexion of uninjured FDL tendons. Gliding Resistance was calculated based on the changes in MTP Flexion Angle over the range of applied loads with higher Gliding Resistance indicating impaired gliding function. Following gliding assessment, tendons were released from the tarsal tunnel, the tibia and calcaneus were removed, and the repaired tendon underwent tensile testing as previously described [4,5]. Briefly, the toes and the proximal end of the tendon were secured in opposing custom grips in an Instron 8841 uniaxial testing system (Instron Corporation, Norwood, MA) and tested in tension at a rate of 30mm/min, until failure. Structural (stiffness, max load at failure, energy to max force and yield load) and material (modulus, strength) outcome parameters were calculated from the plotted force-displacement curves. Cross-sectional area (CSA) of the scar tissue was measured at three places along the length of the

scar tissue that correspond approximately to the middle, and proximal/ distal thirds of the tissue. The average CSA was calculated from these three measurements.

Statistical Analyses:

To identify significant differences in STV over time in C57BL/6J mice, a one-way Analysis of Variance (ANOVA) with Bonferroni post-hoc multiple comparisons were used. Student t-tests were used to identify significant differences between WT and S100a4$^{GFP/+}$ repairs, as well as changes in CSA, echogenicity, modulus and strength between C57Bl/6J repairs at D14 and D28. Significance was set at $p<0.05$. Two independent blinded observers performed all subjective readings (*e.g.* segmentation of STV, assessment of gliding function). Univariate regression analysis was used to determine if STV measured from ultrasound images correlated with gliding function or structural and material properties. To evaluate intraoperator and interoperator error in the segmentation of STV, two operators measured 10 randomly selected C57BL/6J specimens. The average percent error was calculated as the absolute difference between measures divided by the average measurement. The coefficient of variance was calculated as previously described [14]. Percent error was also calculated between STV quantified from segmentation of histology and ultrasound in the same specimens. Interclass correlation coefficients were calculated for both individual observers and between observers. The intraobserver ICC was 0.921 for observer 1 and 0.896 for observer 2. The interobserver ICC was 0.906, indicating a high degree of reliability both for a given observer and between observers.

Results

Segmentation and quantification of Scar Tissue Volume from ultrasound images

To determine whether tendon healing could be measured non-invasively using ultrasound, C57BL/6J mice underwent complete transection and repair of the Flexor Digitorum Longus (FDL) tendon, and ultrasound imaging was performed at 7, 14, 20, and 28 days post-surgery. High-frequency ultrasound permits the identification of the healing (Figure 1C) FDL tendon in 2D sagittal B mode images. From these images, discreet tissues can be segmented on each 2D slice (Figure 1D), including native tendon (pink), bone (green), skin (yellow) and scar tissue (blue). Following segmentation, tissues were reconstructed in 3D (Figure 1E), and Scar Tissue Volume (STV) was quantified (Figure 1E'). The average percent error between operators' measurements was 15.6%, while the coefficient of variation was 16.6%.

Histological validation of US segmentation of STV

To confirm that US image segmentation for volumetric measurement was accurately identifying scar tissue we analyzed 3D reconstructions of histological and US images from the same specimens and observed comparable morphology when segmenting images from both modalities. In addition, volumetric quantification of STV between modalities was highly consistent with a 10.8% error between US and histology segmentation. Taken together, these data suggest our ability to properly identify and segment scar tissue via US imaging (Fig. 2A–H).

Scar Tissue Volume is strongly correlated with end-point metrics of gliding function

No detectable scar tissue was observed in un-injured tendons. At day 7 post-surgery average STV was 0.96 ± 0.158mm^3, with a subsequent increase on day 14 (1.29 mm^3 ± 0.10). Peak STV was observed at day 20 (1.55 mm^3 ± 0.19) with a significant decrease observed at day 28 (0.91 mm^3 ± 0.07), relative to day 20 ($p<0.05$) (Figure 3A). To determine the relationship between STV and metrics of gliding function, univariate linear regression analyses were performed. When day 14 and 28 data were grouped, a significant inverse correlation was observed between STV and MTP Flexion Angle ($R^2=0.70$, $p=0.0002$) (Figure 3B), while a significant, positive correlation was observed between STV and Gliding Resistance ($R^2=0.63$, $p=0.0007$) (Figure 3C). However, when each timepoint was analyzed separately, stronger correlations were observed between STV and gliding function at Day 14 and weaker, non-significant correlations were observed at day 28. At Day 14, a strong, significant inverse correlation was observed between STV and MTP Flexion Angle ($R^2=0.82$, $p=0.005$), while a strong, significant positive correlation was observed between STV and Gliding Resistance ($R^2=0.71$, $p=0.01$). At Day 28 weak, non-significant correlations were observed between STV and MTP Flexion Angle ($R^2=0.46$, $p=0.09$) and Gliding Resistance ($R^2=0.36$, $p=0.15$) (Table 1). Taken together, these data suggest that STV is a significant indicator of gliding function during the earlier phases of tendon healing, but not during later healing.

Scar Tissue Volume does not predict structural or material properties

To determine the potential relationship between STV and tensile mechanical properties, univariate linear regression analyses of STV and tensile mechanical properties (Stiffness, Maximum load at failure, Energy to maximum force and Yield Load) were conducted. When days 14 and 28 were grouped there were no significant correlations between STV and Stiffness ($R^2=0.13$, $p=0.19$) (Figure 4A), Max load ($R^2=0.05$, $p=0.68$) (Figure 4B), Energy to max ($R^2=0.02$) (Figure 4C), or Yield load ($R^2=0.07$) (Figure 4D). Furthermore, no significant associations were observed when each time-point was analyzed separately (Table 1), although moderately strong but non-significant associations were observed between STV and Stiffness at D14 ($R^2=0.54$, $p=0.06$), and STV and Yield load at D14 ($R^2=0.55$, $p=0.054$).

While a trending decrease in Cross-sectional area was observed from D14 to D28, this was not statistically significant ($p=0.15$) (Figure 5A). No significant correlation was observed between CSA and STV at 14 and 28 days ($R^2=0.051$, $p=0.43$) (Figure 5B). Significant increases in modulus (+461%, $p=0.013$) and strength (+361%, $p=0.0049$) were observed between D14-D28, however, no significant correlations were observed between STV and modulus ($R^2=0.003$, $p=0.83$) or strength ($R^2=0.0007$, $p=0.97$) (Figure 5C–F). In addition, no change in echogenicity was observed between D14 and D28 (Figure 5G), and there was no significant association between echogenicity and STV ($R^2=0.02$, $p=0.61$) (Figure 5H).

STV identifies differences in models of fibrotic vs. regenerative healing

We have recently demonstrated that S100a4 haploinsufficiency (S100a4$^{GFP/+}$) results in improved gliding function and mechanical properties, relative to wildtype (WT) littermates [15]. To demonstrate the potential of STV to identify regenerative versus fibrotic models of tendon healing, MTP flexion angle, GR and STV were quantified at day 14 post-surgery in

S100a4$^{GFP/+}$ and WT repairs. Consistent with our previous studies, substantial improvements in gliding function were observed in S100a4$^{GFP/+}$ repairs, including a 93% increase in MTP Flexion Angle (p=0.002) (Figure 6A), and a 62% decrease in Gliding Resistance (p=0.0062) (Figure 6B). A significant 27% decrease in STV was observed in S100a4$^{GFP/+}$ tendons, relative to WT (p=0.0053) (Figure 6C). Taken together, these data suggest that STV has the sensitivity to non-invasively identify functional differences between modes of healing.

Discussion

Following injury, tendons are prone to a fibrotic, scar mediated healing process that both impairs restoration of range of motion and hinders the reacquisition of normal mechanical properties. Given that there are currently no biological approaches to improve the tendon healing process, there is a massive need for increased pre-clinical screening and identification of potential therapies. To address this, we have identified Scar Tissue Volume (STV) as a non-invasive ultrasound metric to determine the effects of genetic or pharmacological modifications on the healing process, which may allow more rapid identification of tendon therapeutics. Importantly, this approach has the potential to dramatically decrease the number of animals needed, consistent with the goals of reducing the number of animals used in biomedical research [16]. Moreover, non-invasive, longitudinal ultrasound imaging can promote more rapid, cost-effective and high-throughput screening to facilitate the identification of therapeutic targets.

Several studies have previously demonstrated the potential of using ultrasound to non-invasively image and assess tendons during mechanical loading [17,18] and tendinopathy [19,20]. In addition, there is strong evidence for the ability of ultrasound to non-invasively assess aspects of the tendon healing process. Ghorayeb *et al.*, quantified extracellular matrix content and found a strong correlation between ECM content and linear stiffness in the Achilles tendon, although changes in range of motion were not assessed. In the current study, we did not observe a significant association between STV and tissue stiffness, although there was a moderately strong relationship at day 14 (R^2=0.54). While quantification of ECM and STV may be similar in that both metrics are likely related to tissue size or bulk, which are associated with impairments in range of motion, differences in correlation with stiffness between ECM and STV may be due to differences in the tissues that were quantified for ECM and STV, timing of analysis, or models of healing. In addition, Yeh *et al.*, used high frequency ultrasound Doppler imaging to assess microcirculation changes, and suggests the potential to determine treatment efficacy using this technique [21]. In contrast to quantification of tissue content or volume, several studies have examined the relationship between ultrasound echogenicity and healing. Tamura *et al.*, used US echogenicity to assess healing in equine Superficial Digital Flexor Tendons, although no change in echogenicity was observed despite longitudinal improvements in strain [22]. Consistent with this, we did not observe any differences in echogenicity between 14 and 28 days post-surgery. In contrast, Lee *et al.*, assessed the relationship between US echogenicity, and tensile mechanical properties in a collagenase-induced tendinopathy model and demonstrated that echo intensity was positively correlated with maximum strain and

stiffness [23], suggesting that echogenicity changes may be more pronounced during tendinopathy development, relative to acute tendon healing.

An important aspect of this approach is the ability to detect functional differences related to tendon ROM non -invasively and over time. However, gait analysis can also be used to non-invasively assess restoration of function during tendon healing [24–26]. While gait analysis is a strong metric in assessing Achilles and supraspinatus tendon healing in pre-clinical models, it is not yet known how alterations in gait correspond to flexor tendon healing phases. Moreover, gait analysis parameters are typically associated with measurements of pain and weakness, while the relationship between gait and tissue morphology is unknown. While we observe changes in STV over the course or healing, these differences are relatively modest, with no differences in STV observed between 14- and 20-days post-surgery. While we typically observe only slight differences in gliding function metrics between these time-points [4], it is also likely that there are additional factors contributing to the decreased utility of STV at later time-points, such as changes in ECM composition and alignment, as well as integration between the native tendon and scar tissue. Consistent with this, Riggins *et al.*, used high-frequency ultrasound to assess collagen organization [27], suggesting the potential to combine volumetric and morphological assessment using ultrasound. Importantly, the real utility of endpoint metrics of gliding function is in identifying differences between genetically different strains of mice [8], or between pharmacological treatment groups [15] at a given timepoint. Taken together, these data strongly suggest that longitudinal US based quantification of STV may be utilized as a corollary to predict tendon ROM and gliding function during healing.

While STV strongly correlates with gliding function, there are several limitations to this study that must be considered. STV does not correlate with structural or material properties, which are critical indicators of the value of a particular therapeutic intervention. Thus, future work seeks to develop multiple US-based metrics which either alone or using multi-variate analyses may better correlate with restoration of structural and material properties. Addition of metrics that reflect or predict these changes will enhance the utility of non-invasive ultrasound imaging to assess tendon healing. Furthermore, we have only assessed healing in S100a4$^{GFP/+}$ and WT mice at Day 14. However, we have confined our analysis in these animals to day 14 due to the decrease in predictive power of STV at day 28. In addition, the scalability of this metric to larger pre-clinical models, or clinical US has yet to be determined, as has the ability to identify and quantify scar tissue using lower resolution clinical ultrasound machines. Finally, while the goal of developing longitudinal, non-invasive metrics of healing is to permit relatively rapid and cost-effective therapeutic target screening, the segmentation process requires substantial expertise and is quite time-consuming, thus, to make this approach more high-throughput we will need to semi-automate or automate the segmentation process.

Here we have shown that Scar Tissue Volume is significantly correlated with end-point metrics of gliding function, and STV is particularly predictive of gliding function at Day 14, the period of peak impairments in gliding function. In addition, STV is sensitive enough to discriminate between phenotypically distinct models of healing. Future work will develop additional US-based metrics with the goal of non-invasive estimation of structural and

material properties. Taken together, this study identifies quantification of Scar Tissue Volume using longitudinal, non-invasive ultrasound imaging as a novel means to assess tendon healing. This approach may permit the rapid screening of biological and pharmacological interventions for healing, and identify promising therapeutic targets, in an efficient, cost-effective manner.

Supplementary Material

Refer to Web version on PubMed Central for supplementary material.

Acknowledgements

We would like to thank the Histology, Biochemistry and Molecular Imaging (HBMI) and the Biomechanics, Biomaterials and Multimodal Tissue Imaging (BBMTI) Cores for technical assistance. Research reported in this publication was supported by the National Institute of Arthritis and Musculoskeletal and Skin Diseases of the National Institutes of Health under Award Numbers K01 AR068386, R01 AR073169, R21 AR073961 and P30 AR069655. The content is solely the responsibility of the authors and does not necessarily represent the official views of the National Institutes of Health.

References

1. Langer R & Vacanti JP. 1993 Tissue engineering. Science 260, 920–926. [PubMed: 8493529]
2. de Jong JP, Nguyen JT, Sonnema AJ. et al. 2014 The incidence of acute traumatic tendon injuries in the hand and wrist: a 10-year population-based study. Clinics in orthopedic surgery 6, 196–202. [PubMed: 24900902]
3. Aydin A, Topalan M, Mezdegi A. et al. 2004 [Single-stage flexor tendoplasty in the treatment of flexor tendon injuries]. Acta Orthop Traumatol Turc 38, 54–59. [PubMed: 15054299]
4. Loiselle AE, Bragdon GA, Jacobson JA. et al. 2009 Remodeling of murine intrasynovial tendon adhesions following injury: MMP and neotendon gene expression. J Orthop Res 27, 833–840. [PubMed: 19051246]
5. Hasslund S, Jacobson JA, Dadali T. et al. 2008 Adhesions in a murine flexor tendon graft model: Autograft versus allograft reconstruction. J Orthop Res 26, 824–833. [PubMed: 18186128]
6. Tanaka T, Amadio PC, Zhao C. et al. 2003 Gliding resistance versus work of flexion--two methods to assess flexor tendon repair. J Orthop Res 21, 813–818. [PubMed: 12919868]
7. Zhao C, Ettema AM, Berglund LJ. et al. 2011 Gliding resistance of flexor tendon associated with carpal tunnel pressure: a biomechanical cadaver study. J Orthop Res 29, 58–61. [PubMed: 20661935]
8. Loiselle AE, Frisch BJ, Wolenski M. et al. 2012 Bone marrow-derived matrix metalloproteinase-9 is associated with fibrous adhesion formation after murine flexor tendon injury. PloS one 7, e40602. [PubMed: 22792383]
9. Ackerman JE, Best KT, O'Keefe RJ & Loiselle AE. 2017 Deletion of EP4 in S100a4-lineage cells reduces scar tissue formation during early but not later stages of tendon healing. Sci Rep 7, 8658. [PubMed: 28819185]
10. Spinella G, Britti D, Loprete G. et al. 2016 Relative Echogenicity of Tendons and Ligaments of the Palmar Metacarpal Region in Foals from Birth to 4 Months of Age: A Longitudinal Study. PloS one 11, e0159953. [PubMed: 27441630]
11. Suydam SM & Buchanan TS. 2014 Is echogenicity a viable metric for evaluating tendon properties in vivo? Journal of biomechanics 47, 1806–1809. [PubMed: 24726653]
12. Callis G & Sterchi D. 1998 Decalcification of Bone: Literature Review and Practical Study of Various Decalcifying Agents. Methods, and Their Effects on Bone Histology. Journal of Histotechnology 21.
13. Schneider CA, Rasband WS & Eliceiri KW. 2012 NIH Image to ImageJ: 25 years of image analysis. Nat Methods 9, 671–675. [PubMed: 22930834]

14. Reynolds DG, Shaikh S, Papuga MO. et al. 2009 muCT-based measurement of cortical bone graft-to-host union. Journal of bone and mineral research : the official journal of the American Society for Bone and Mineral Research 24, 899–907.
15. Ackerman JE, Nichols AE, Studentsova V. et al. 2019 Cell non-autonomous functions of S100a4 drive fibrotic tendon healing. eLife 8.
16. Flecknell P. 2002 Replacement, reduction and refinement. ALTEX 19, 73–78.
17. Bogaerts S, De Brito Carvalho C, Scheys L. et al. 2017 Evaluation of tissue displacement and regional strain in the Achilles tendon using quantitative high-frequency ultrasound. PloS one 12, e0181364. [PubMed: 28727745]
18. Chimenti RL, Flemister AS, Ketz J. et al. 2016 Ultrasound strain mapping of Achilles tendon compressive strain patterns during dorsiflexion. Journal of biomechanics 49, 39–44. [PubMed: 26655590]
19. Chimenti RL, Bucklin M, Kelly M. et al. 2016 Insertional achilles tendinopathy associated with altered transverse compressive and axial tensile strain during ankle dorsiflexion. J Orthop Res
20. Malliaras P, Purdam C, Maffulli N & Cook J. 2010 Temporal sequence of greyscale ultrasound changes and their relationship with neovascularity and pain in the patellar tendon. Br J Sports Med 44, 944–947. [PubMed: 19139035]
21. Yeh CK, Chen JJ, Li ML. et al. 2009 In vivo imaging of blood flow in the mouse Achilles tendon using high-frequency ultrasound. Ultrasonics 49, 226–230. [PubMed: 18835004]
22. Tamura N, Nukada T, Kato T. et al. 2017 The use of sonoelastography to assess the recovery of stiffness after equine superficial digital flexor tendon injuries: A preliminary prospective longitudinal study of the healing process. Equine veterinary journal 49, 590–595. [PubMed: 28083881]
23. Lee SY, Chieh HF, Lin CJ. et al. 2017 Characteristics of Sonography in a Rat Achilles Tendinopathy Model: Possible Non-invasive Predictors of Biomechanics. Sci Rep 7, 5100. [PubMed: 28698601]
24. Howell K, Chien C, Bell R. et al. 2017 Novel Model of Tendon Regeneration Reveals Distinct Cell Mechanisms Underlying Regenerative and Fibrotic Tendon Healing. Sci Rep 7, 45238. [PubMed: 28332620]
25. Wang Z, Liu X, Davies MR. et al. 2018 A Mouse Model of Delayed Rotator Cuff Repair Results in Persistent Muscle Atrophy and Fatty Infiltration. Am J Sports Med, 363546518793403.
26. Bell R, Taub P, Cagle P. et al. 2015 Development of a mouse model of supraspinatus tendon insertion site healing. J Orthop Res 33, 25–32. [PubMed: 25231092]
27. Riggin CN, Sarver JJ, Freedman BR. et al. 2014 Analysis of collagen organization in mouse achilles tendon using high-frequency ultrasound imaging. J Biomech Eng 136, 021029. [PubMed: 24356929]

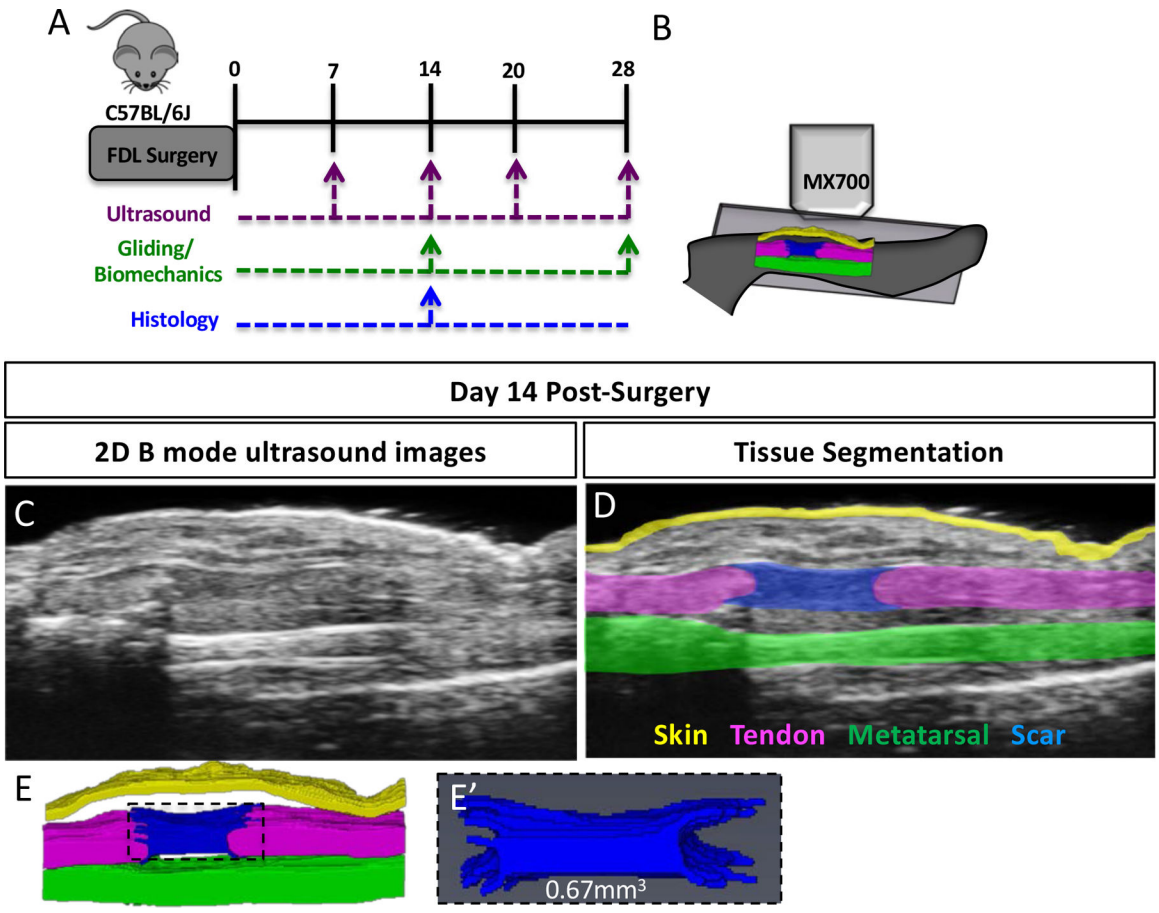

Figure 1. Quantification of Scar Tissue Volume from ultrasound images.

(A) Experimental design for longitudinal ultrasound assessment of tendon healing at 7, 14, 20- and 28-days post-surgery, followed by assessment of gliding function at day 28. An additional cohort of animals underwent ultrasound imaging only at day 14, followed by either histological analysis, or assessment of gliding function. (B) Schematic of ultrasound setup showing sagittal plane of imaging. (C) 2D B Mode ultrasound image of a healing tendon at day 14 post-surgery. (D) Segmentation of skin (yellow), metatarsal (green), FDL tendon (pink) and scar tissue (blue) at day 14 post-surgery. (E) 3D Reconstruction of segmented tissues at day 14 post-surgery. (E') 3D reconstruction and volumetric quantification of STV at day 14 post-surgery.

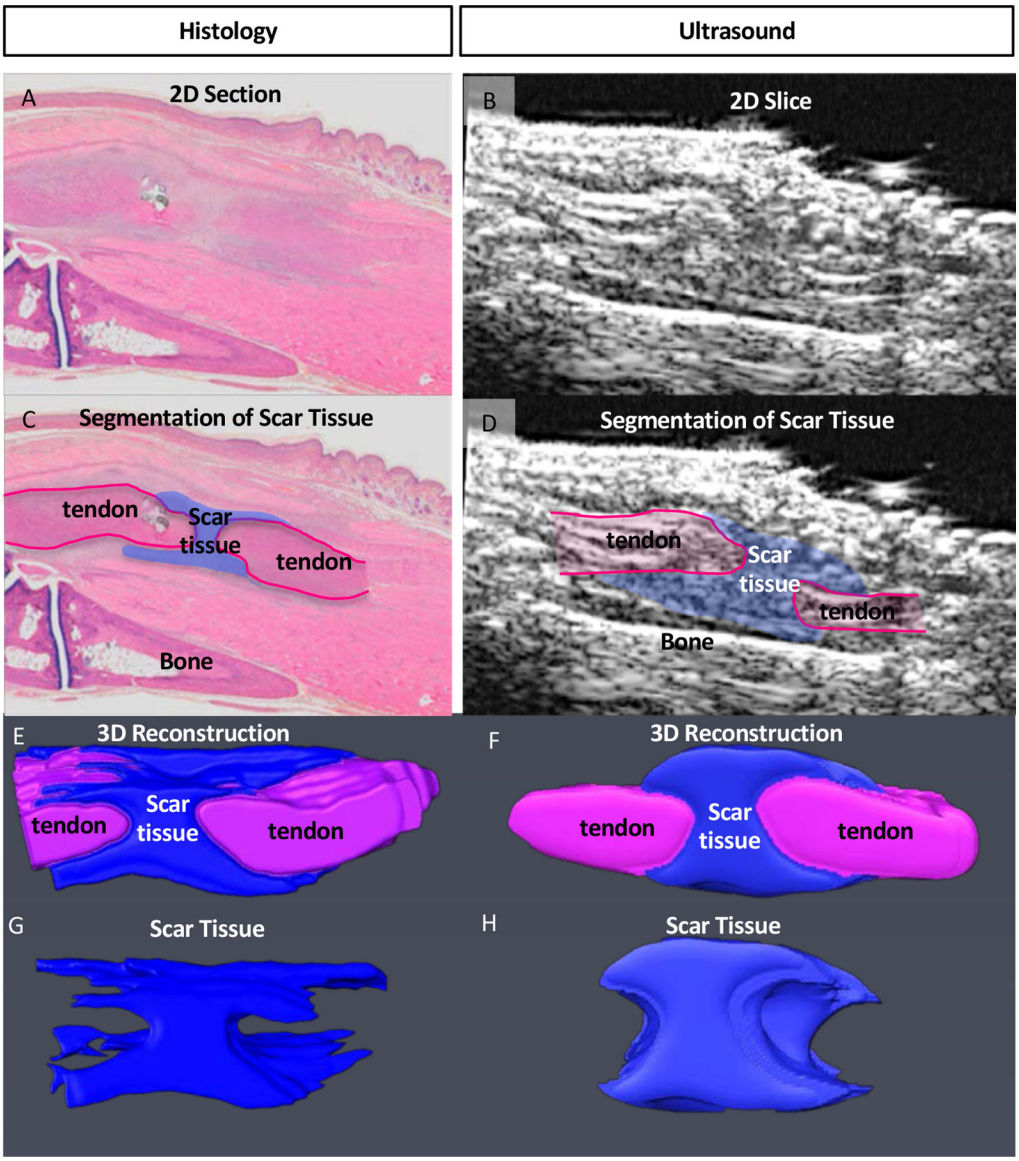

Figure 2. Validation of Scar Tissue Segmentation using histology.

(A & B) 2-Dimensional sagittal Histological (A) and US (B) image sections from the same specimen. (C & D) Segmentation of scar tissue (blue) and tendon (pink) from (C) histology, and (D) US images. (E & F) Following segmentation of all 2D images containing scar tissue from (E) histology, and (F) US, the segmented slices were reconstructed in 3D, and (G & H) scar tissue was volumetrically quantified.

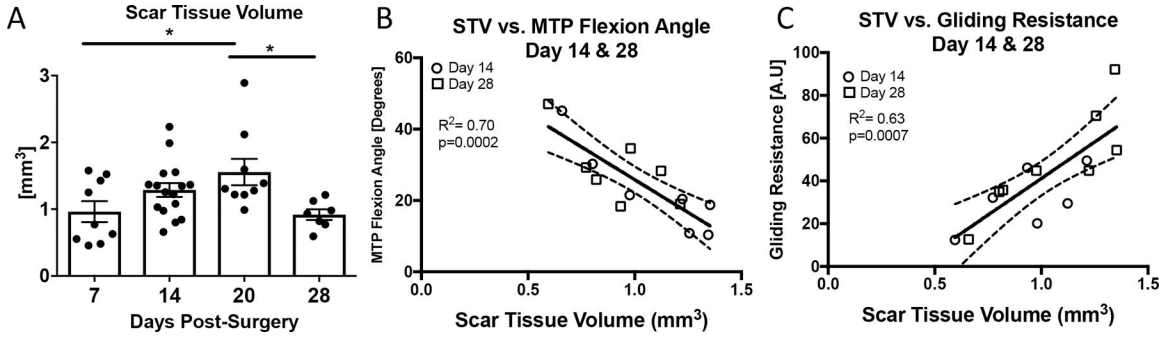

Figure 3. Scar Tissue Volume is correlated with changes in gliding function.

(A) Scar Tissue Volume was quantified longitudinally at 7, 14, 20, and 28 days post-surgery. Peak STV was observed at day 20. (*) indicates $p<0.05$. (B-C) Linear regression analyses of STV and (B) MTP Flexion Angle, (C) Gliding Resistance at 14 and 28 days. White circles represent day 14 and grey squares represent day 28.

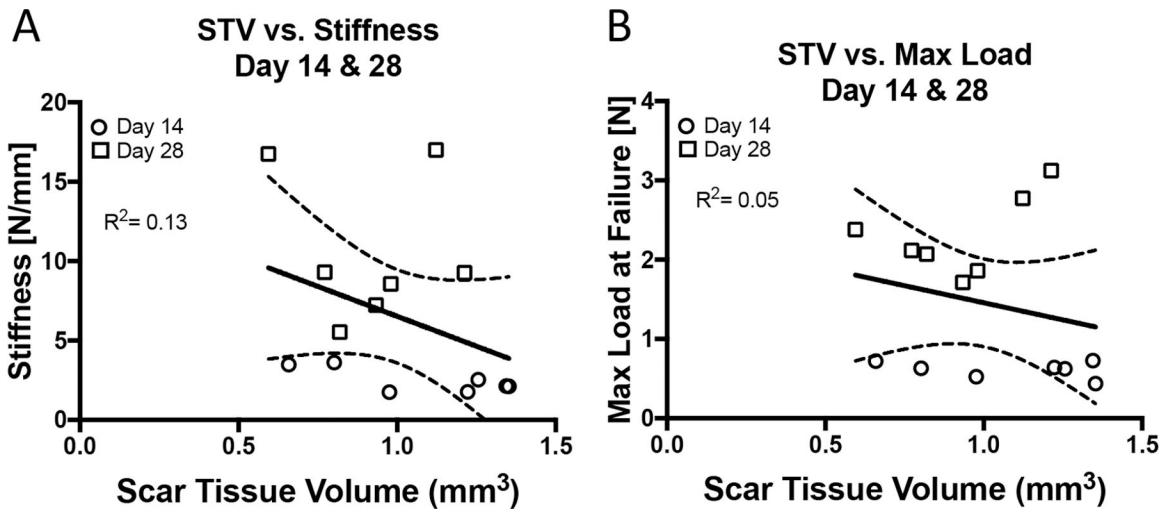

Figure 4. Scar Tissue Volume is not correlated with tensile mechanical properties.

Linear regression analyses of STV and (A) Stiffness, (B) Max load at failure, (C) Energy to maximum load, (D) Yield load at 14, and 28 days post-surgery. White circles represent day 14 and grey squares represent day 28.

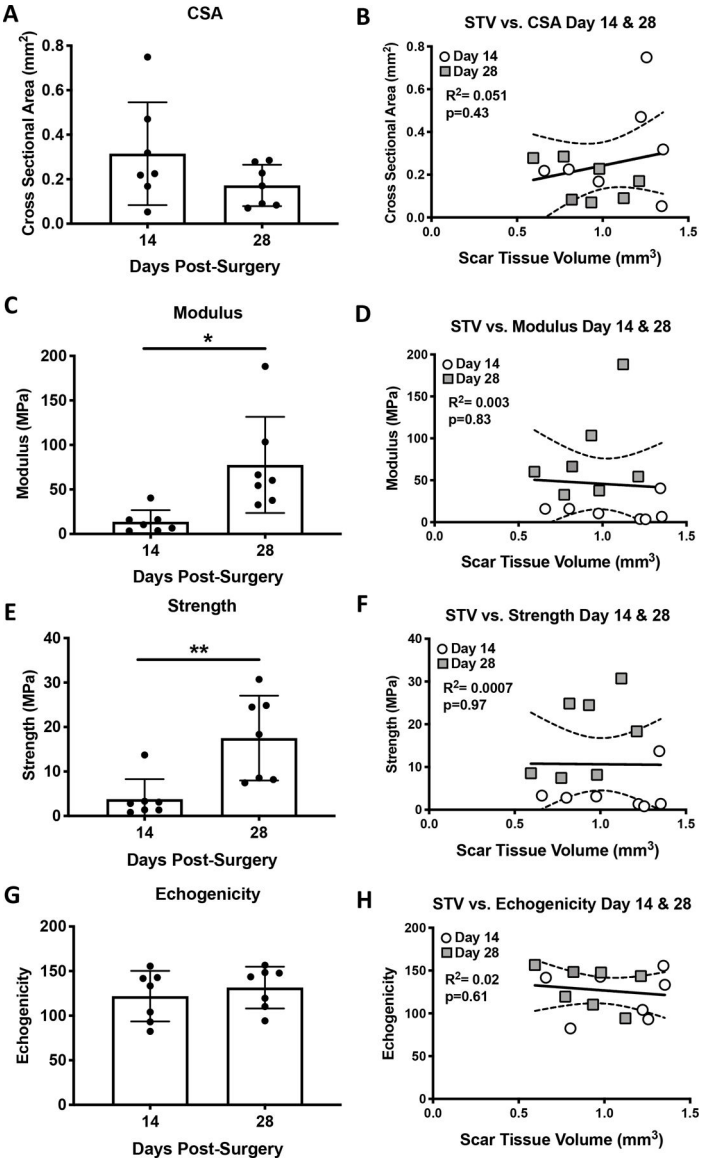

Figure 5. Scar Tissue Volume is not correlated with CSA, echogenicity or material properties.

Cross sectional area (A), Modulus (C), Strength (E) and Echogenicity (G) were quantified at 14 and 28 days post-surgery, and correlated with STV using linear regression analyses (B, D, F, H). White circles represent day 14 and grey squares represent day 28.

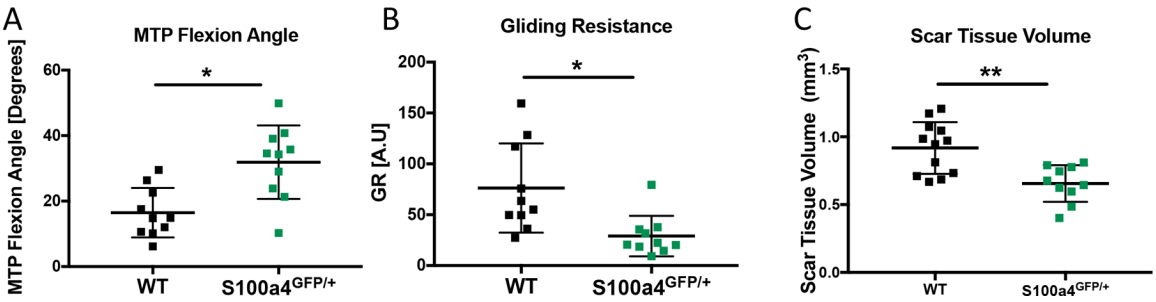

Figure 6. Scar Tissue Volume identifies functional differences between models of scar-mediated and regenerative tendon healing.

Quantification of A) MTP Flexion Angle, B) Gliding Resistance and C) Scar Tissue Volume in WT and S1004 haploinsufficient ($S100a4^{GFP/+}$) tendon repairs at day 14 post-surgery. $S100a4^{GFP/+}$ mice heal with improved gliding function and decreased STV. (*) indicates $p<0.05$, (**) indicates $p<0.001$.

Table 1.

Correlations between Scar Tissue Volume and parameters of gliding function, structural and material properties at 14- and 28-days post-surgery.

	Scar Tissue Volume			
	Day 14		**Day 28**	
	r	**p value**	**r**	**p value**
Gliding Resistance	0.71**	0.01	0.36	0.15
MTP Flexion Angle	0.82**	0.005	0.46	0.09
Stiffness	0.54	0.06	0.009	0.83
Max load at failure	0.09	0.49	0.25	0.24
E to Max Force	0.20	0.31	0.15	0.38
Yield Load	0.55	0.054	0.18	0.33
CSA	0.08	0.52	0.23	0.26
Echogenicity	0.01	0.82	0.14	0.39
Modulus	0.0009	0.94	0.15	0.38
Strength	0.04	0.63	0.25	0.24